analyses, as reported previously.[1] Anal. Calcd for $C_{10}H_9O_{10}P_1Na_4{\cdot}4H_2O$: C, 24.80; H, 3.54; P, 6.40. Found: C, 24.52; H, 3.60; P, 6.38.

S3P was prepared for NMR studies by passing the sample over Dowex 50 (Na^+ form). The samples were pH adjusted, concentrated in vacuo, and exchanged (3×) with 2-mL aliquots of demineralized D_2O (Merck MSD). Final samples were at least 50 mM in S3P and 1 μM EDTA. The pK_a of the second ionization of the phosphate group was previously determined to be 6.41.[21] The EPSP ketal NMR samples were prepared similarly to the S3P samples. Solutions were subjected to three freeze–thaw cycles and then sealed in the NMR tubes. All pH's reported are adjusted for D_2O activity. Proton spectra are referenced to 3-(trimethylsilyl)-1-propanesulfonic acid sodium salt, TSP, (0.0 ppm) in D_2O as a secondary standard.

^1H NMR spectra were recorded at 300 or 400 MHz. Both spectrometers were equipped with 15-bit analogue to digital converters. 1D spectra were acquired using the selective inversion recovery experiment with on-resonance and off-resonance acquisitions interleaved. For all resonances except H_4 and H_5, selective 180° pulses (49 ms) were employed in the selective inversions. Due to the smaller chemical shift difference between H_4 and H_5, 100° pulses (27.2 ms) were used for selective inversions. The total recycle time employed was 5 s, comprised of a 4-s preparatory delay and a 1-s acquisition time. Mixing times of intermediate values, 200–600 ms, were employed with the maximum number of transients per block set to 1000. In general, a minimum of three mixing times were employed for each proton examined. NOESY spectra were acquired using the standard three-pulse experiment in the phase-sensitive mode.[22] Suppression of the HOD resonance was not used for S3P due to the close proximity (2–10 Hz) of H_3 to HOD. The 2D data sets were zero filled to 2K by 2K and weighted in both dimensions by 75° shifted sinebell functions. Base-line correction was used in ω_1 and drift correction in ω_2. Volume integrations were used to quantitate the observed NOE's.

T_1 values for S3P were determined by the inversion-recovery method and at 300 MHz: H_2 (2.78 s), H_3 (1.07 s), H_4 (1.82 s), H_5 (1.51 s), H_{6e} (0.68 s), and H_{6a} (0.64 s). On the basis of the ratio of T_1's at 300 and 400 MHz the overall correlation time, τ_c,[23] was approximated to be 110 ps. The EPSP ketal T_1 values at 400 MHz are: H_2 (2.12 s), H_3 (1.17 s), H_4 (1.45 s), H_5 (1.25 s), H_{6e} (0.40 s), H_{6a} (0.36 s), and CH_3 (0.56 s).

NOE distances were obtained by averaging the experimental cross-relaxation rates for each H–H interaction. The diastereotopic geminal protons at C_6 provide an internal standard for determining H–H distances, and for these geminal protons it is take to be 1.8 Å and is not expected to vary as a function of pH. In general, for the 1D analysis, the average cross-relaxation rate was derived from six data points, three mixing times taken from two different inversion experiments. 2D analysis followed from single data sets taken in the region where the NOE build-up was linear. The magnitude of the analyzed NOE's ranged from 0.5–10%. SIRNOE data sets for S3P at pH 5.04, 7.00, and 9.25 and the EPSP ketal at pH 7.00 were collected at 300 MHz. NOESY spectra were obtained at 400 MHz for the EPSP ketal at pH 10.0 and for S3P at pH 7.0.

Acknowledgment. We acknowledge Mr. William C. Hutton (Monsanto), who collected preliminary NMR data on S3P solutions. We would also like to thank Professor Niels H. Andersen of the University of Washington and Dr. Michael J. Miller (Monsanto) for their helpful discussions.

Supplementary Material Available: Complete tables of molecular mechanics energies, calculated H–H distances and coupling constants for conformers of 1 and 2, and ^1H chemical shifts for 1 at varying pH (6 pages). Ordering information is given on any current masthead page.

(21) Castellino, S.; Leo, G. C.; Sammons, R. D.; Sikorski, J. A. *Biochemistry* **1989**, *28*, 3856–3868.
(22) States, D. J.; Haberkorn, R. A.; Ruben, D. J. *J. Magn. Reson.* **1982**, *48*, 286–292.
(23) Mirau, P. A.; Bovey, F. A. *J. Am. Chem. Soc.* **1986**, *108*, 5130–5134.

Theoretical Studies in Molecular Recognition: Asymmetric Induction of Benzophenone Imine Ester Enolates by the Benzylcinchoninium Ion

Kenny B. Lipkowitz,* Michael W. Cavanaugh, Brian Baker, and Martin J. O'Donnell*

Department of Chemistry, Indiana University–Purdue University at Indianapolis, 1125 E. 38th Street, Indianapolis, Indiana 46205

Received September 5, 1990 (Revised Manuscript Received May 24, 1991)

Molecular-recognition techniques are used to examine the complexes formed between a chiral phase-transfer catalyst and enolates that are known to be alkylated enantioselectively. The ion pairs have well-defined, albeit flat, intermolecular potential energy surfaces that show binding regions consistent with a proposed model. The influence of dispersion vs Coulomb forces on these potential energy surfaces is addressed as is the origin of enantiofacial selectivity. An energy-partitioning algorithm that statistically weights intermolecular interaction energies for all orientations of the two molecules in the complex is used to determine which fragments of the cinchoninium ion are most responsible for enolate binding. The roles other molecular fragments play, on both the catalyst and the enolate, for ion pairing are examined.

Introduction

In an earlier paper one of us reported the enantioselective synthesis of α-amino acids by phase-transfer catalysis (PTC).[1] In contrast to most other asymmetric syntheses of amino acids that use stoichiometric amounts of chiral auxiliaries, this method involves using catalytic quantities of the enantiocontrol element. Under the PTC conditions moderately high levels of enantiomeric excess (ee) were obtained using a chiral catalyst and a prochiral protected glycine derivative 1. This prochiral substrate meets two important criteria for successful synthesis of α-amino acids: it undergoes monoalkylation under PTC conditions and, once alkylated, it is not easily racemized during reaction or workup. The catalysts used as asymmetric templates are derived from the cinchona alkaloid family 2.

(1) O'Donnell, M. J.; Bennett, W. D.; Wu, S. *J. Am. Chem. Soc.* **1989**, *111*, 2353–2355.

0022-3263/91/1956-5181$02.50/0

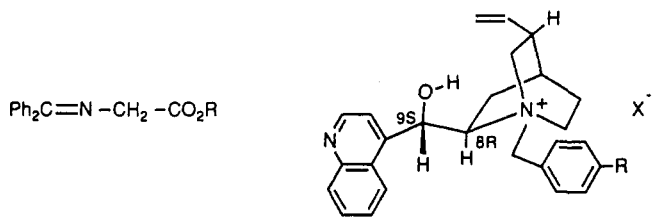

1 2

The PTC process for alkylation of the active methylene compound 1 is outlined in Figure 1.[2] The first step of the process involves deprotonation at the interface by base to generate the benzophenone imine enolate. This enolate is transported into the organic phase by coordinating as an ion pair with a quaternary ammonium ion that then reacts with the electrophile. The step prior to alkylation, in which the enolate and ammonium ions associate, is the critical step for asymmetric induction and is the focus of this paper. It is necessary to know where the enolate binds to the catalyst and how the cinchoninium ion acts as a chiral template. With this understanding it will be possible to predict which functional group or groups or other regions of the molecule could be modified to enhance asymmetric induction. This process is the first step in computer-assisted molecular design (CAMD) of enantioselective PTC synthesis.

In this paper the molecular recognition processes responsible for asymmetric alkylation will be studied. The following questions will be addressed: Where does the enolate bind on the catalyst? What are the forces holding the ion pair together? What is the most likely configuration of the enolate? What is the origin of facial selectivity that gives rise to asymmetric alkylation?

Experimental Section

1. Computational Tools. The molecular mechanics calculations were done with the MM2 force field.[3] In some parts of this work the MMX force field[4] as implemented in PCMODEL[5] or the MM2-85 force field as implemented in MACROMODEL[6] are used. The conformational analysis was done as explained in the following paragraph. Throughout this paper all calculations assumed a dielectric constant of 1.5 unless stated otherwise and no cut-offs of any kind were invoked. The MM2 bond moments were replaced with atomic charges derived from semiempirical molecular orbital theory using the AM1 Hamiltonian[7] in MOPAC.[8] All quantum mechanical calculations assumed a ground-state singlet species and convergence was achieved in all cases. Geometry optimizations using MOPAC were done with the "Precise" command to ensure proper minimization as suggested by Boyd et al.[9] The molecular mechanics energy minimizations were done with the block-diagonal Newton Raphson method followed by a full-matrix Newton Raphson optimization so that the gradient root mean square < 0.1 kJ/Å mol. The molecular dynamics calculations were done with MACROMODEL as described below. Calculations were done on a VAX 8850 mainframe computer or a Silicon Graphics workstation. Specialized software written in-house will be described in the text.

2. Conformer Searching. Four methods were adopted for locating conformers. In order of ascending complexity they are as follows: manual searching, grid searching, simulated annealing, and quenched dynamics.

(a) Manual searching involved setting important torsion angles (vide infra) close to what was believed to be minimum energy values based on mechanical models and chemical intuition. It can be argued that chemical intuition is more sophisticated than the other methods used but it contains an inherent bias by the operator that can lead to incorrect conclusions. Consequently, these studies were supplemented with automated computer searches.

(b) In the second method, grid searching, slices through the multidimensional potential energy surface were generated by using the double dihedral driver option of MM2.[3] Pairs of important torsion angles were swept from 0° to 340° in 20° increments to reconstruct the multidimensional surface. Bond lengths and bond angles were not optimized during these searches. The minima located by the rigid body search were then fully optimized.

(c) The third method used was simulated annealing.[10] Simulated annealing is one of the few optimization algorithms capable of locating a global minimum by itself. It is a relatively new technique only now being implemented by organic chemists and has been described by others.[11] The rate at which the system cools is referred to as the annealing schedule and is critical for successful location of the global minimum.[12] By lowering the temperature too quickly the annealing process is speeded up, but, as in crystallization, it is possible to end up in a metastable state. In this study, four distinct cooling schedules were used: one fast, one short, and two intermediate. Furthermore, three distinctly different conformational states on the hypersurface were used initially to ensure the same results irrespective of initial conditions. The incremental rotation allowed for each degree of freedom was 15°, but in some trials the rotations were constrained to 5° increments. The simulated annealing algorithm as implemented in PCMODEL was used. Here, the MMX force field from Serena Software was used in place of the MM2 force field.

(d) The final conformer searching method used was quenched molecular dynamics. The MD criteria are described below; here only the method of searching for conformers is explained. Beginning with different starting conformations obtained earlier, the ion was warmed from 0 to 1000 K over a 5-ps time period. The ion was coupled to a 1000 K bath temperature to retain this artificially high temperature, and the simulation was run for 20 ps, collecting samples every 0.5 ps. These structures were then energy minimized (quenched) with 250 steps of a block diagonal Newton Raphson optimizer. If the resulting energies looked promising they were further minimized for comparison with other structures. Structures were accepted as new conformers if their rms deviation of all atoms ≥ 0.700 Å when compared to other known conformations.

3. Molecular Dynamics. The dynamics simulations were carried out with MACROMODEL beginning with the fully optimized, lowest energy structure located by the other searching techniques. The following options were used for all simulations: timestep = 0.001 ps; dielectric = 1.5; nonbonded cutoff = 20 Å; electrostatic cutoff = 20 Å; hydrogen bond cutoff = 20 Å. The nonbonded atom list was updated every 0.001 ps, but 0.0001 ps for the high-temperature-quenched dynamics runs. Initial kinetic energy was added to all atoms as random velocities. Translational and rotational momentum was reset to zero every 0.5 ps during all simulations. To maintain a constant temperature, the system was coupled to an external temperature bath. For the quenched dynamics this bath was set at 1000 K. For the production runs of the simulation reported later in this paper the bath was set at 300 K. Coupling between bath and molecule was updated every 0.2 ps.

The MD simulations used the MM2 force field and the AMBER force field as implemented in MACROMODEL. For these simulations the global minimum located by the conformer searching was

(2) Rabinovitz, M.; Cohen, Y.; Halpern, M. *Angew. Chem., Int. Ed. Engl.*, **1986**, *25*, 960–970.
(3) Allinger, N. L. *J. Am. Chem. Soc.* **1977**, *99*, 8127–8134.
(4) Gajewski, J. J.; Gilbert, K. E.; McKelvey, J. In *Advances in Molecular Modeling*; JAI Press: Greenwich, 1990; Vol. 2.
(5) Serena Software, Box 3076, Bloomington, IN, 47402-3076.
(6) Mohamadi, F.; Richards, N. G. J.; Guida, W. C.; Liskamp, R.; Lipton, M.; Caufield, C.; Chang, G.; Hendrickson, T.; Still, W. C. *J. Comput. Chem.* **1990**, *11*, 440–467.
(7) Dewar, M. J. S.; Zoebisch, E. G.; Healy, E. F.; Stewart, J. J. P. *J. Am. Chem. Soc.* **1985**, *107*, 3902–3909.
(8) Stewart, J. J. P., MOPAC Version 4, Quantum Chemistry Program Exchange Bulletin, *3*, 455.
(9) Boyd, D. B.; Smith, D. W.; Stewart, J. J. P.; Wimmer, E. *J. Comput. Chem.* **1988**, *9*, 387–398.
(10) Kirkpatrick, S.; Gelatt, C. D.; Vecchi, M. P. *Science* **1983**, *220*, 671–680.
(11) Wilson, S. R.; Cui, W.; Moskowitz, J. W.; Schmidt, K. W. *Tetrahedron Lett.* **1988**, *29*, 4373–4376.
(12) Bounds, D. G. *Nature (London)* **1987**, *329*, 215–19.

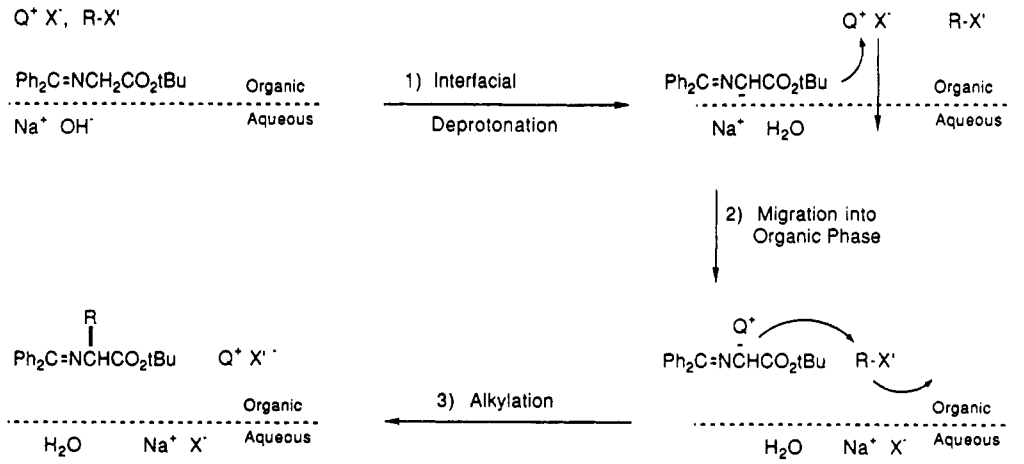

Figure 1. Mechanism of phase-transfer catalysis.[2]

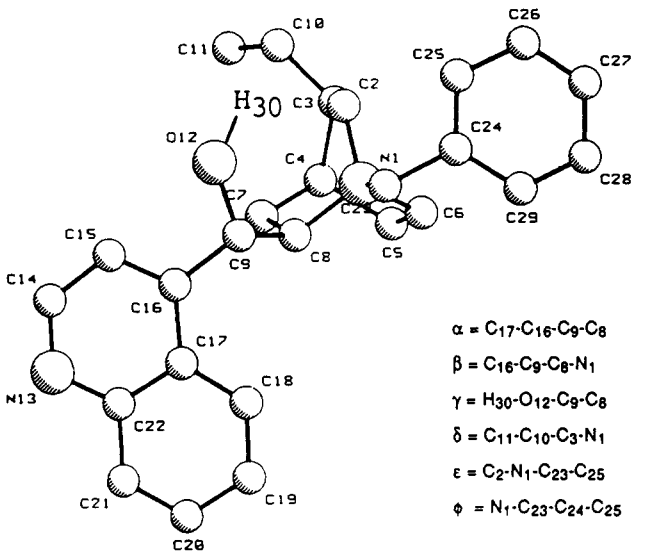

Figure 2. X-ray structure of *N*-benzylcinchoninium chloride (halide omitted and H_{30} added manually) with definitions of torsional angles $\alpha - \phi$.

warmed from 0 to 300 K over a 1-ps time period and then equilibrated at 300 K for 5 ps. The production runs were for 50 ps each. Structures were sampled every 1 ps and saved for analysis.

Results and Discussion

I. Structures of Ions. A. Catalyst. First the conformational states accessible to the catalyst **2** were considered. The calculations were done without consideration of solvent and without the bromide ion. Hence, these calculations are of an isolated gas-phase ammonium ion with a net charge of +1. The bromide ion was omitted because the major concern was with the inherent conformational properties of the catalyst itself. In the following section the counter ion (enolate) is explicitly included in the calculations.

The important torsion angles are defined according to the atom-numbering scheme presented in Figure 2. This conformation, as shown, is from an unpublished X-ray crystallographic study[13a] of *N*-benzylcinchoninium chloride and, as such, corresponds to a static structure in the solid state. From the combined conformational searching methods a large number of stable conformations were found, relatively few of which are within 4 kcal mol^{-1} of the global minimum. These low-energy structures are compiled in Table I.

Table I. Summary of MM2 Steric Energies of Low-Energy Conformations for Catalyst 2

steric energies (kcal mol^{-1})	torsion angles (deg)					
	α	β	γ	δ	ε	φ
36.6	75.2	179.7	-179.7	-160.1	-63.6	93.1
36.7	74.6	179.8	179.9	-94.6	-63.6	92.8
37.1	75.4	-179.3	-179.8	-6.8	-64.8	93.1
37.7	75.3	178.9	-179.0	91.7	-63.6	93.3
38.5	72.5	175.4	-179.4	-91.3	-169.8	83.6
40.2	74.5	178.9	-176.5	-97.5	53.0	118.4
40.8	-93.5	-180.0	172.2	-92.8	-63.4	92.7
40.8	-92.6	179.9	172.5	179.0	-63.6	93.0
41.0	73.7	-174.2	79.8	-92.2	-63.7	92.6
41.1	-91.6	179.5	172.5	-6.4	-63.6	93.0
41.2	174.1	-169.7	170.0	-179.6	-65.3	90.8
41.3	165.0	-159.7	-175.4	-17.8	-175.5	92.3
41.4	176.1	-171.8	170.2	-93.2	-65.1	92.2
41.7	125.1	-71.4	-174.5	178.2	-65.2	94.2
41.7	174.1	-169.9	172.0	-23.3	-65.2	90.5
42.2	-97.7	-177.8	170.6	175.6	-167.3	90.1
42.2	125.3	-71.8	-174.5	-6.3	-65.2	-92.0
42.2	125.3	-71.8	-174.5	-6.3	-65.2	94.3
42.4	-55.6	-67.1	-174.3	-97.4	-67.1	93.1
42.9	-55.1	-70.0	-175.2	-6.1	66.6	93.1
43.4	68.9	179.4	79.2	-29.5	-172.2	80.6

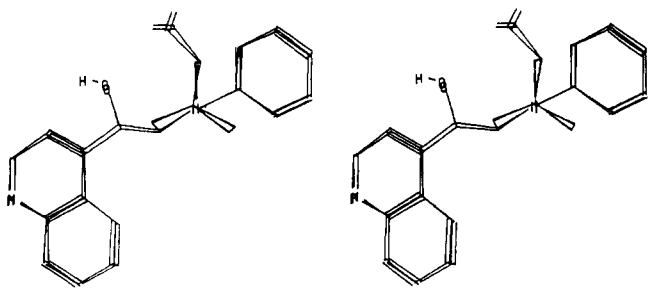

Figure 3. Stereoview of the least-squares fit of *N*-benzylcinchoninium ion X-ray with MM2. Note the displacement of the vinyl group.

The most salient features of Table I are that, while the calculated global minimum is quite similar to the X-ray structure, it is not exactly the same and that there exist several conformers of similar energy whose structures differ only by rotation around torsion angle δ. It is expected, especially for flexible molecules like **2**, that lattice forces will distort the molecule one way or another along the potential energy surface near the global minimum. The

(13) (a) Dolling, U.-H.; Hughes, D. L.; Springer, J. P. Unpublished X-ray data. (b) Hughes, D. L.; Dolling, U.-H.; Ryan, K. M.; Schoenewaldt, E. F.; Grabowski, E. J. J. *J. Org. Chem.* **1987**, *52*, 4745–4752.

relationship between the X-ray structure (which has been subsequently minimized by MM2) and the lowest energy conformer located from the search methods is shown in Figure 3 where the quinuclidine rings have been superimposed by a least-squares fitting of the eight heavy atoms. The main difference between these structures involves torsion angle δ, which in the solid state is $-115°$ but in gas or liquid phases is expected to be $-160°$. The energy difference between these two conformations is only 0.40 kcal mol^{-1}, which is easily overcome by lattice forces.[14] Consequently, the benzylcinchoninium ion adopts a more compact, folded shape in the crystal than that expected in the gas or liquid phases.

Although the orientation of the vinyl group is inconsistent with that of the X-ray structure, the remaining torsion angles are nearly coincident. These torsion angles are especially important because they define the relative spatial positioning of the aryl rings with respect to the quinuclidine ring. It has been suggested that the quinoline and benzyl rings are coplanar and orthogonal to the local 3-fold axis of the quinuclidine when enolate ions bind.[13b] Both the X-ray and molecular mechanics results are supportive of this idea. While the two aromatic rings can librate (see dynamics results in supplementary material) they are, at their minimum, almost flat with an interring angle between the planes equal to 24° (10° X-ray). This creates a platform where the enolate, acting as a substrate docking to a receptor, can bind. In the following sections this is discussed further.

B. Enolates. For the enolate ions described below, only the naked anion itself, without counterion and solvent, is considered. Later, the structural features of both the catalyst and the enolates in the presence of one another are addressed.

Seven benzophenone imine enolates (**3–9**) and the phenylindanone enolate (**10**) reported by the Merck group[13b] were studied. It is noted that these benzo-

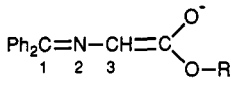

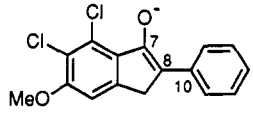

10

3 R = $C(CH_3)_3$
4 R = CH_3
5 R = $CH(CH_3)_2$
6 R = CH_2CH_3
7 R = $C(CH_2CH_3)_3$
8 R = $CH_2C(CH_3)_3$
9 R = $CHPh_2$

phenone imine anions can exist as *E* or *Z* enolates[15] (**11** and **12**), and both diastereomeric forms were considered.

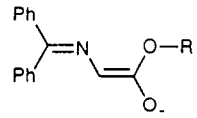

11 (E-enolate)

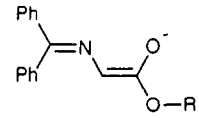

12 (Z-enolate)

Conformer searching was done as described in the preceding section. For most cases the conformational structures and energies that were located by molecular mechanics were corroborated by semiempirical molecular orbital theory. The results are presented in the supplementary material as Tables SI–SVII, where MM and QM energies (of the lowest energy structures only) along with pertinent torsion angles are listed. A noteworthy finding is that the *E* enolate (**11**) is more stable than the *Z* enolate

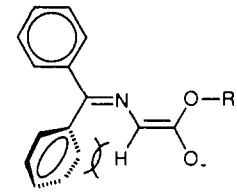

11

(**12**). If a small metal ion like lithium had been included in the calculation the *Z* enolate would be more stable.[16] These small ions can associate with both the N and O^- atoms simultaneously to stablize the *Z* form by orbital interactions and/or coulombic attractions. For large ammonium counter ions, which have a diffuse charge distribution, it is unlikely that such chelation of the enolate is important. Initially, only the inherent conformations of the enolate by itself are of interest. Later the shape of the enolate in the ion pair will be considered.

One question from the outset of this study involved the shape of the benzophenone portion of the enolate. The results of these calculations show both rings to be twisted out of plane but not equally. The phenyl group cis to the vinyl hydrogen is rotated out of plane 30–50° while the trans phenyl is canted ~10–20° depending on the computational method employed. The origin of the large twisting of the cis phenyl group is purely steric, arising from the interaction of the enolate vinyl hydrogen with the ortho hydrogen on the phenyl group.[17] The computed twisting in the benzophenone portion of the enolate is consistent with the ring twisting of the parent ethyl ester **6** as well as the monophenylated product **13**, both of which have been determined by X-ray crystallography[18] (Figure 4).

The ester portion of the enolate is where most of the conformational mobility takes place. For the simple esters like Me, Et, *i*-Pr, and *t*-Bu there are relatively few conformational states accessible at ambient temperatures for both the *Z* and *E* enolates. For the ester groups $-CH_2C(CH_3)_3$, $-CH(Ph)_2$ and $-C(Et)_3$ there were a substantial number of thermally accessible conformational states. In the following section, as a starting point, only the lowest energy conformers of the *Z* and the *E* enolates are used. Later, other conformations are considered by dynamic averaging.

II. Catalyst–Enolate Binding Site. Binding sites in biological systems like proteins or nucleic acids have well-defined cavities, crevices, or clefts to which a substrate may bind. Unlike biological systems whose binding sites are often defined by concave topologies, in the present study the surface topology of the catalyst is convex, giving rise to an ill-defined binding site. Nonetheless, before assessing *how* the enolate binds to the catalyst it is necessary first to address *where* it binds. Because there is no well-defined cavity or cleft into which the enolate can dock the word "binding site" will be avoided and the term "binding region" will be used to describe where around the cinchoninium ion the enolate spends most of its time.

One approach to describing the binding region is to compute the molecular electrostatic potential (MEP)[19] of

(14) Murray-Rust, P. *Molecular Structures and Biological Activity*; Griffin, J. F., Duax, W. L., Eds.; Elsevier: New York, 1982.
(15) Evans, D. A. In *Asymmetric Synthesis*; Morrison, J. D., Ed.; Academic Press: New York, 1984; Vol. 3, Chapter 1.
(16) See ref 15 for numerous examples of similar chelated enolates.
(17) For a review of related allylic 1,3-strain, see: Hoffmann, R. W. *Chem. Rev.* **1989**, *89*, 1841–1860.
(18) O'Donnell, M. J.; Bennett, W. D.; Jacobsen, W. N.; Ma, Y.-a.; Huffman, J. C. *Tetrahedron Lett.* **1989**, *30*, 3909–3912.

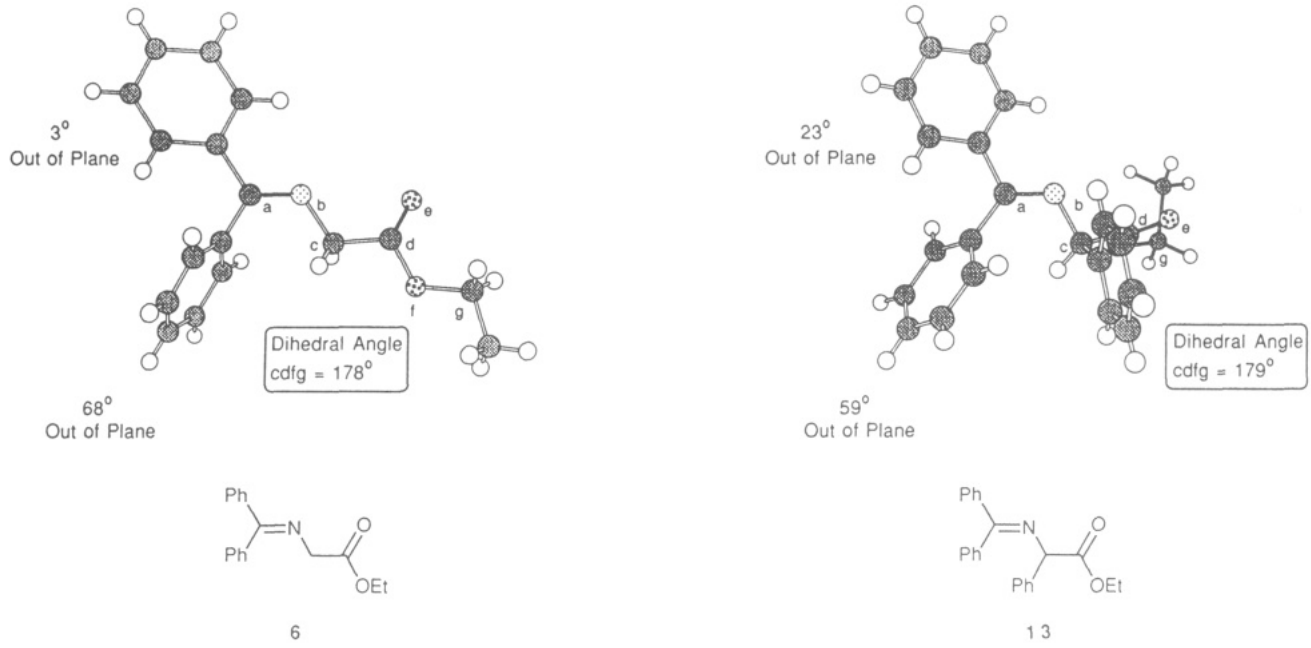

Figure 4. X-ray crystal structures of compounds **6** and **13** to demonstrate twisting of phenyl groups and C=C—O—R torsion angles in imines.

the catalyst. This would indicate where favorable and unfavorable regions around the catalyst exist for association of a negative point charge. The problem with this approach is that while the enolate has a charge of −1 this charge is not a point charge. Rather, it is delocalized over large parts of the molecule. Furthermore, the binding process involves more than simple electrostatics; clearly dispersion forces, π-stacking, and hydrogen bonding will complement the long-range Coulomb forces holding the complexes together. Consequently, the enolate itself will be used as a probe molecule to determine the low-energy binding region around the cinchoninium ion. The methodology used follows.

a. Methodology. The lowest energy structures of the cinchoninium ion and the enolates are used initially, admitting that these structures will change upon complexation. Nonetheless, these rigid body structures are good initial probes of the intermolecular potential energy surface. First an origin and axis system are selected for all ions. For the benzophenone enolates (**3–9**) the origin is centered on N_2, the X axis lies along the N_2–C_1 bond, and C_3 lies in the XY plane. For the Merck enolate (**10**) the origin is C_8, the X axis lies along the C_8–C_{10} bond, and C_7 is in the XY plane. For the *N*-benzylcinchoninium ion (**2**) the origin is the ammonium nitrogen N_1. The X axis is along the N_1–C_{23} bond and atom C_2 lies in the XY plane. In all cases the Z axis is orthogonal, using a right-hand coordinate system, to the XY plane.

The position of the enolate with respect to the catalyst is given in a polar coordinate system, r, θ, ϕ where r is the distance between origins and θ and ϕ are the latitude and longitude, respectively, of the enolate (Figure 5). At each latitude, θ, and longitude, ϕ, around the catalyst a large number of Euler angles defining the relative orientation of the two molecules are considered. For each Euler angle at a given θ and ϕ the van der Waals surfaces are allowed to just touch and an intermolecular energy is computed. For each Euler angle, then, r will vary. A large number of orientations of enolate are computed for each value of

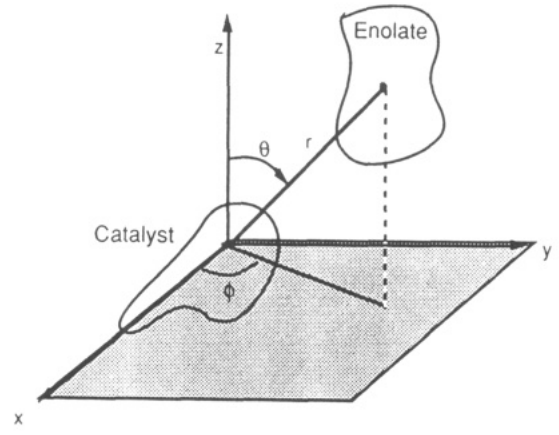

Figure 5. Position of enolate with respect to the chiral catalyst in spherical coordinates (r, θ, ϕ). The origin on the catalyst is the quaternary ammonium nitrogen. The axes are defined in the text.

θ and ϕ. The Euler angles are selected so that a uniform sampling of enolate orientations are evaluated, i.e., not just the two faces of the enolate. In this study each enolate probe is moved, in 10° increments, from θ = 0° to 360° and ϕ = 0° to 180°. Thus, all parts of the surface of the catalyst are being probed with all possible orientations of the enolate. Details of this computational method have been published.[20]

In essence, the enolate is being rolled over the van der Waals surface of the catalyst looking for low-energy binding regions. Each rolling motion considered ~155 000 unique orientations of enolate around the catalyst. At each latitude, θ, and longitude, ϕ, the lowest energy structure is selected and its energy plotted as a function of position. An example is presented in Figure 6. Contour maps of the intermolecular potential energy surfaces for all enolates can be found in the supplementary material. These plots are the minimum-energy intermolecular potential energy

(19) Mezey, P. G. In *Reviews in Computational Chemistry*; Lipkowitz, K. B., Boyd, D. B., Eds.; VCH Publishers: New York, 1990; Chapter 7.

(20) Lipkowitz, K. B.; Demeter, D. A.; Zegarra, R.; Larter, R.; Darden, T. *J. Am. Chem. Soc.* **1988**, *110*, 3446–3452. The derivation of equations used and extension of this algorithm for studies in molecular recognition exist: Blanco, M. *J. Comput. Chem.* **1991**, *12*, 237–47.

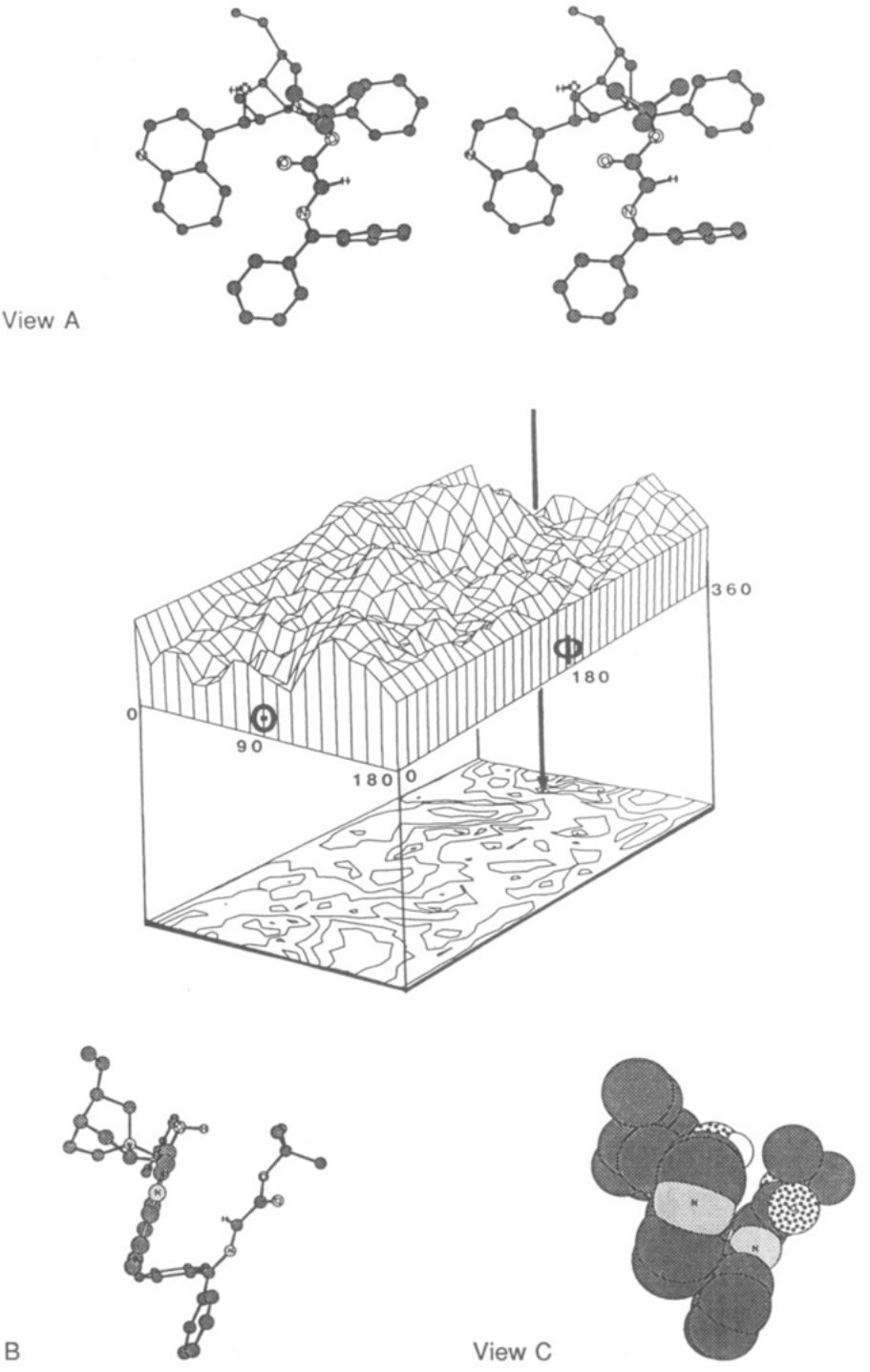

Figure 6. Two- and three-dimensional potential energy surfaces for the complex formed between *Z* enolate **3** and cinchoninium ion **2**. View A is a stereoview of the enolate–catalyst complex at the global minimum (the N_1–C_2 bond is on the *Y* axis and atoms N_1, C_2, and C_6 of catalyst **2** are in the *XY* plane). Views B and C are ball-and-stick and space-filling models, respectively, of the complex shown in A after a 90° rotation about the *Y* axis.

surfaces. Since each enolate is different it was necessary to probe each potential energy surface using each enolate as a unique test probe.

b. *Z* Enolates. It is seen that the intermolecular energy surfaces are very flat and ill-defined. This contrasts with a similar study where the binding region around Rebek's cleft was probed and found to contain well-defined and deep minima for substrate binding.[21] The reason for such flat surfaces is that a large component of the cohesive interaction between enolate and catalyst arises from dispersion forces as well as electrostatic attractions (vide infra). These dispersion forces are favorable for all θ and ϕ. Furthermore, the electrostatic attractions are somewhat washed out because of the highly delocalized anion along with a cation whose charge is itself well dispersed. The charges for the *tert*-butyl ester, as an example, are shown in Figure 7. It should be noted that the carbon and hydrogen atoms bearing most of the positive charge of the catalyst are at some distance from the ammonium nitrogen itself.[22] Although this combination of effects leads to

(21) Lipkowitz, K. B.; Zegarra, R. *J. Comput. Chem.* **1989**, *10*, 595–602.

(22) Reetz, M. T. *Angew. Chem., Int. Ed. Engl.* **1988**, *27*, 994–998.

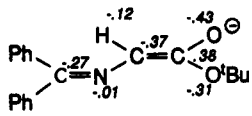

3 (E-enolate)

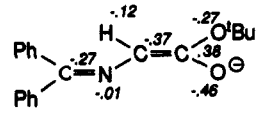

3 (Z-enolate)

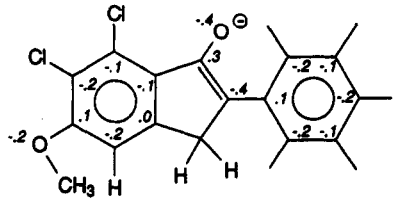

10 (Merck Enolate)

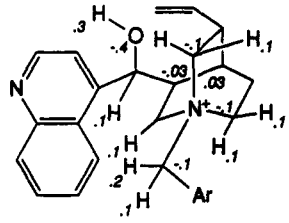

2 (N-Benzylcinchoninium Ion)

Figure 7. Distribution of charge density in enolates 3 and 10 and catalyst 2. Not all charges are shown for clarity.

shallow minima on the intermolecular energy surfaces as depicted, there is one key feature they all display. They all indicate low-energy binding regions around $\theta = 70°–80°$ and $\phi = 330°–10°$. This region corresponds to front-side binding where front side refers to the face created by the coplanar aromatic rings, i.e., as viewed in Figure 2. This finding is consistent with the proposed mechanism of asymmetric alkylation of the phenylindanone enolate ion by the Merck group.[13b] In all cases the global minima are flat, indicating wide-amplitude sliding motions of enolate are possible.

The topology of the intermolecular surfaces (Figure 6 and supplementary material) arises from both dispersion (Lennard-Jones) and Coulomb forces. It was of interest to determine how dominant a role the Coulomb forces play in defining the topology of these surfaces. To study this, several calculations were repeated with all atomic charges set to zero, leaving only the dispersion terms active. While there are some differences, generally the intermolecular potential energy surfaces with and without charges look similar. The major differences are the depths of the minima, which are deeper when coulomb terms are turned on. These results are consistent with the earlier observation that the charges on both the catalyst and the enolates are highly delocalized, resulting in a washed out coulombic interaction. It appears that dispersion forces alone are capable of binding the enolates in a productive, front-side manner. The coulomb interactions appear only to give more definition to the intermolecular surfaces by deepening the minima. Consequently, it is suggested that coulombic attractions hold the ion pair together tightly but that dispersion forces are mainly responsible for the topology of the intermolecular surfaces, which in turn allow for front-side enolate binding.

c. *E* Enolates. A similar analysis has been carried out for the *E* enolates. The intermolecular potential energy surfaces (not shown) are similar to those found for the *Z* enolates above. These surfaces generally have low-energy binding regions around $\theta = 70–100°$ and $\phi = 320–20°$. Again, this corresponds to front-side association but these minima are quite shallow, allowing for easy transits from one point on the surface to another. Generally, the global minima on the *E* enolate surfaces are less well-defined and more scattered than those on the *Z* enolate.

d. Merck Enolate. The procedure used for the *Z* and *E* enolates described above was next used for the phenylindanone enolate. The structure of this enolate was determined quantum mechanically. Only one conformation was located and, as expected, it is planar with a well-dispersed charge. The intermolecular potential energy surface for this ion pair (Figure 8) is similar to that in Figure 6 with the global minimum at $\theta = 130°$ and $\phi = 260°$. However, the contour lines for this ion pair are, in general, more closely spaced, and the energy differences between minima and maxima are larger than those in Figure 6. These findings are consistent with the Merck interpretation of a mechanism involving tight ion pairing.[13b]

Overall, then, a preference is observed for front-side association of all enolates with the *N*-benzylcinchoninium ion. The minimum energy binding regions on the intermolecular potential surfaces are broad and shallow, implicating wide-amplitude sliding motions for all ion pairs. Generally, but not always, the *Z* enolate surfaces have lower minima than the *E* enolates. The attractive forces responsible for holding the ion pair together will be addressed later, but here it is seen that the resonance delocalization of enolate charge coupled with the diffuse nature of the ammonium ion give rise to ill-defined binding regions in the ion pairs.

III. Facial Selectivity. The goal of this research is to examine how and why asymmetric induction takes place when benzophenone imine enolate esters are alkylated in the presence of the *N*-benzylcinchoninium ion. The alkylation transition states[23] for *si*- and *re*-face alkylation should be modeled because these transition states reflect the relative rates of alkylation that result in the asymmetric induction. However, it is not known what these transition states look like nor is there certainty about the *Z*–*E* configuration of the enolates (vide infra). Rather than model the actual transition structures, the point along the reaction coordinate that precedes the transition state, i.e., the ion pair prior to alkylation, has been modeled. It is assumed here that the intermolecular forces preferentially stabilizing one of the two transition states are also responsible for facial selectivity in the ion pair. Several key points need to be emphasized. Firstly, the electrophile is not accounted for in the modeling study, and it is assumed that the low-energy structures derived from the search strategy (vide infra) are the ones leading to product. This may not be true. Indeed, since the energy differences between many of the complexes are small, it may be that one of the complexes of slightly higher energy has a transition state with a lower energy of activation (Curtin–Hammett principle).[24] Secondly, changing the electrophile does not modify the configuration of the major enantiomer.[1] Thus, in terms of the Curtin–Hammett system, the product ratio P_R/P_S continues to favor the R configuration, independent of the electrophile, suggesting that K_R/K_S remains relatively constant. Further experi-

(23) Lead references for recent studies involving modeling of transition-state structures: (a) Houk, K. N. *Pure Appl. Chem.* **1989**, 643–650. (b) Menger, F. M.; Sherrod, M. J. *J. Am. Chem. Soc.* **1990**, *112*, 8071–75.

(24) (a) Seeman, J. I. *Chem. Rev.* **1983**, *83*, 83–134. (b) Seeman, J. I. *J. Chem. Educ.* **1986**, *63*, 42.

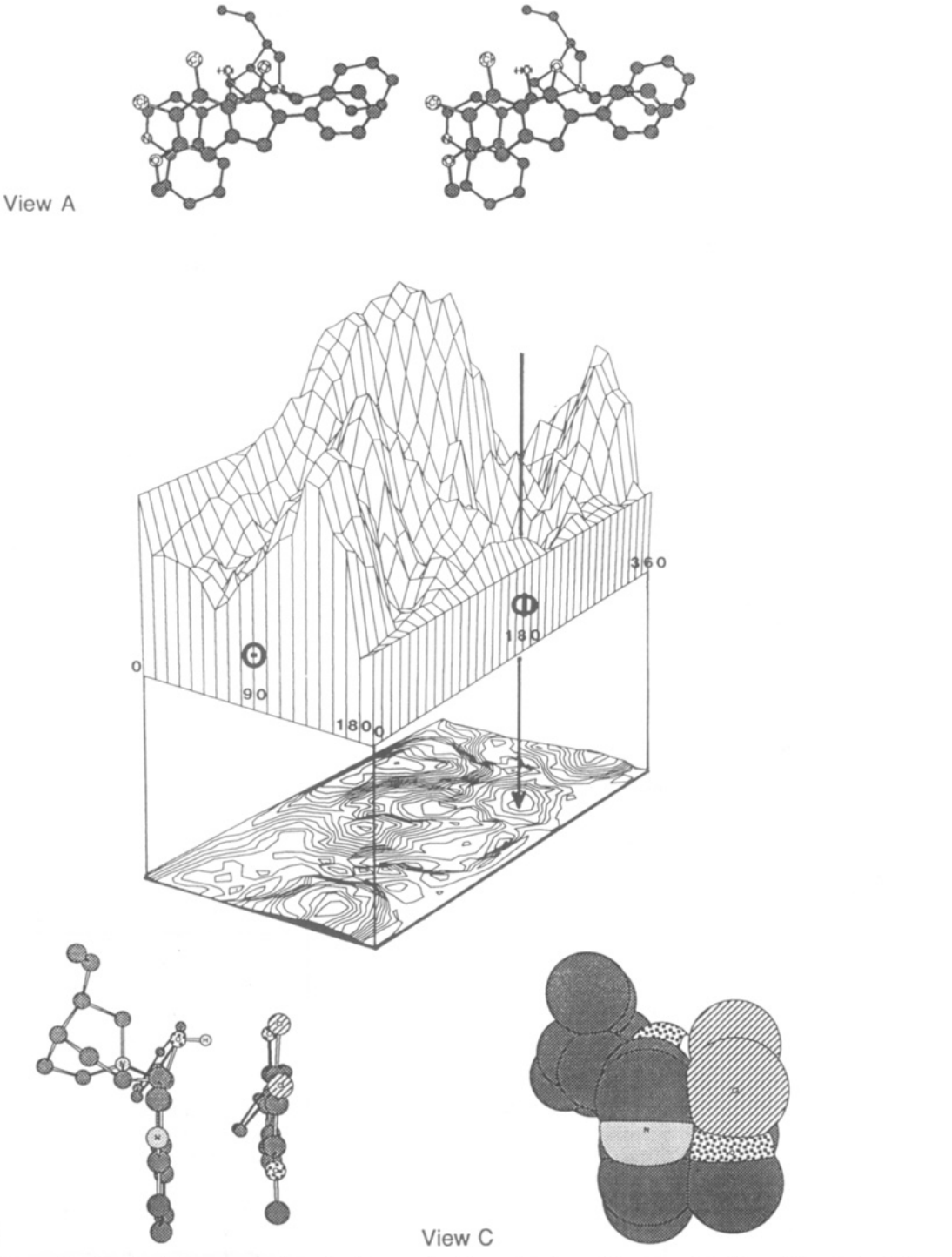

Figure 8. Two- and three-dimensional potential energy surfaces for the complex formed between Merck enolate **10** and the cinchoninium ion **2**. View A is a stereoview of the enolate–catalyst complex at the global minimum (the N_1–C_2 bond is on the Y axis and atoms N_1, C_2, and C_6 of catalyst **2** are in the XY plane). Views B and C are ball-and-stick and space-filling models, respectively, of the complex shown in A after a 90° rotation about the Y axis.

mental and theoretical studies are in progress to clarify the details of this complex reaction system.

Having examined the intermolecular potential energy surfaces, it is now known, approximately, where the enolates prefer to bind to the catalyst. Consequently, one can focus on this binding region to determine the most likely shape of the ion pair prior to electrophilic attack. Stereographic "snapshots" (not shown) for a large number of low-energy enolate orientations near the global minima on the intermolecular surfaces show the plane of the enolate to be parallel with the plane made by the aromatic rings on the catalyst. The two faces of Z or E enolate are designated, by convention, as *si* or *re*.[25] For the E enolate shown, the *re* face is to the front while the *si* face is to the rear (Figure 9). To examine the actual structure of the ion pair, to evaluate how receptor and substrates deform from their lowest energy isolated gas-phase shapes, and to assess which face is preferred, energy minimizations and short molecular dynamics simulations were carried out.

Beginning from the lowest energy $\theta\phi$ point on the intermolecular surface the two ions are minimized as a single supermolecule. This energy is recorded. The original structure of the rigid-body enolate on the $\theta\phi$ surface is then

(25) Hanson, K. R. *J. Am. Chem. Soc.* **1966**, *88*, 2731–2742.

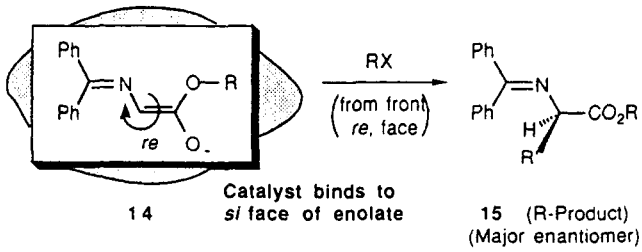

Figure 9. Catalyst–enolate complex demonstrating facial selectivity in binding and alkylation.

Table II. *si* vs *re* Binding Energies (MM2) in kcal mol^{-1} for *E* Enolates 11

enolate	expl % ee[1]	*si* energy	*re* energy	ΔE
3*E*	56	-31.64	-31.40	-0.24
4*E*	30	3.98	-2.92	1.06[a]
5*E*	42	-12.95	-11.57	-1.38
6*E*	36	-5.44	-4.56	-0.88
7*E*	40	4.37	2.34	2.00[a]
8*E*	44	-2.29	-3.85	1.56[a]
9*E*	14	-6.69	-6.34	-0.35

[a] Wrong prediction.

rotated 30° with respect to the catalyst, and the entire structure is minimized again. This process is repeated until all orientations of enolate with respect to catalyst have been sampled, thereby examining all *si*- and *re*-face orientations.

a. *E* Enolates. Using this approach a search was made for the lowest energy ion pair for the *E* enolates described above. The *E* enolates, in the absence of counter ions, are slightly more stable than the *Z* enolates (vide supra). The results of this search are presented in Table II. Note that if the *si* face binds to the catalyst the *re* face is exposed to electrophilic attack. Alkylation from the *re* face is predicted to give rise to *R* product **15**, which is the major enantiomer observed experimentally (Figure 9). Hence, preferential *si*-face binding of enolates takes place during ion pairing.

In Table II, three of the seven examples are incorrectly predicted. Furthermore, the energy differences, ΔE, between the most stable *si* and the most stable *re* structures should correlate with the experimental ee and they don't. These results can be interpreted in several ways: either the theory examined herein does not work or other processes are involved in lowering the enantiomeric excess. These possibilities are discussed later. Another possible explanation is that the *E* enolates do not show a consistent facial selectivity. The answer to this question awaits further experimental evidence.

b. *Z* Enolates. Employing the same methodology as above, a search was made for the lowest energy structures of the ion pairs (Table III). Two important observations are made. First, in all cases *si* facial selectivity is predicted. Second, there is a linear relationship between facial selectivity, ΔE, and experimental ee.[1] This relationship is depicted graphically in Figure 10. The structural features of these low-energy complexes are informative. For example, Figure 6 shows the intermolecular potential energy surface for the *Z* enolate *tert*-butyl ester **3**. Also depicted in this figure is a front-side stereoview of the lowest energy *si*-face structure along with ball-and-stick and space-filling side views. This intermolecular potential energy surface, in contrast to that of the Merck enolate–catalyst complex (Figure 8), is a gently rolling surface with poorly defined maxima and minima. Additionally, as seen in the stereoview, the enolate fits into a groove of the catalyst rather than directly in front of the catalyst as in the Merck enolate case.

Table III. *si* vs *re* Binding Energies (MM2) in kcal mol^{-1} for *Z* Enolates 12

enolate	expl % ee[1]	*si* energy	*re* energy	ΔE
3*Z*	56	-33.12	-31.50	-1.62
4*Z*	30	-0.18	-0.12	-0.06
5*Z*	42	-13.30	-12.57	-0.75
6*Z*	36	-4.11	-3.69	-0.42
7*Z*	40	-4.07	-2.47	-1.60
8*Z*	44	-9.75	-8.40	-1.35
9*Z*	14	-8.21	-8.16	-0.05

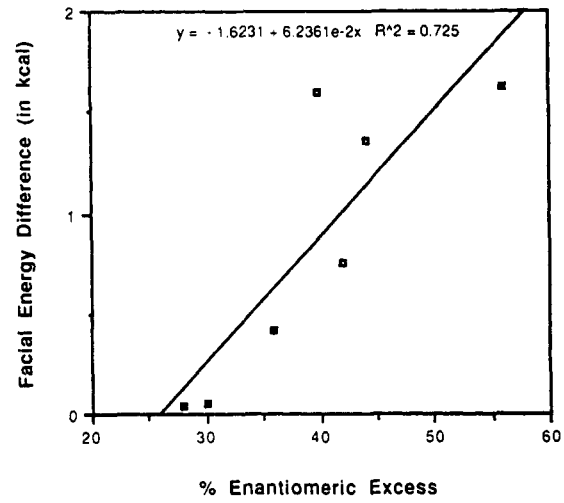

Figure 10. Plot of ΔE, the difference between the most stable *re*- and *si*-face structures, for the *Z* enolates **12** vs experimental enantiomeric excess.

c. Merck Enolate. The same docking strategy implemented for the benzophenone imine ester enolates was adopted for the phenylindanone enolate. Both *si*- and *re*-face binding to the catalyst were computed, and it was found that *si* facial selectivity dominates in the ion pairing. This selectivity is consonant with the observed alkylation results[13b] and is depicted in Figure 8. The three-dimensional potential energy surface shows a mountainous intermolecular potential in which the energy differences between maxima and minima are large and the global minimum is relatively well-defined. It is seen that the preferred orientation of enolate with respect to catalyst is similar to that proposed by the Merck group. Note that the planar enolate rests in front of both aromatic rings of the catalyst and hydrogen bonding along with coulombic forces hold the complex together tightly. Additionally, comparison of the two enolate–catalyst complexes (Figures 6 and 8) shows that the latter involves a much tighter fit of enolate onto the surface of the catalyst, which is likely due to the planar, cyclic structure of the Merck enolate **10**.

The energy difference between the lowest energy *re*- and *si*-face complexes of the Merck enolate, ΔE, is 0.32 kcal mol^{-1}. This number should be larger, given the observed >90% ee; hence, it appears that the global minimum may not have been located for the *si* face of the Merck enolate. An alternative explanation is that experimental evidence exists for a 2:1 ratio of cinchoninium ion to enolate prior to alkylation.[13b] The modeling presented here invokes a 1:1 ratio.

At this point it is necessary to address the reliability of these calculations. The energy differences giving rise to the observed enantioselectivity are quite small (<1 kcal mol^{-1}) and would appear to exceed the ability of the com-

putations. Is there any meaning to such small energy differences? Are the current modeling tools too crude to predict the right answer? Is the energy difference between these complexes lost in the noise? The computed heats of formation for a diverse series of molecules with the MM2 force field gives a standard deviation of 0.42 kcal/mol, which improves to 0.37 kcal/mol when vibrational effects are included.[26] One may argue that the accuracy of molecular mechanics is simply not good enough for modeling systems like these. However, we are comparing virtually identical systems. The standard deviation of 0.37 kcal/mol observed for nonidentical molecules does not apply for identical systems. Indeed, in this study we are comparing the *si* vs the *re* face of the *same molecule*. Hence, the molecular mechanics errors in one diastereofacial complex will be the same as those in the other complex. The near cancellation of errors provides small but meaningful energy differences. Using the same modeling tools and concepts as used here, we have previously computed small energy differences ($<kT$) of enantiomeric analytes binding to chiral surfaces.[27] The double difference cancellation of errors does indeed provide meaningful results! Next, it is noted that while the ion pair is being treated as a single molecule, its potential energy surface is exceedingly, complex with thousands of local minima. Consequently, there is no guarantee that the global minimum has been found; in fact, it is likely that it has not been located. Nonetheless, the calculated global minimum is likely near the real minimum. On a related point, these optimizations originated from the most stable enolate structures calculated in vacuo as isolated molecules. While induced-fit changes of both enolate and catalyst are being considered here, it is possible that larger structural changes that have not been considered could take place upon binding. Overall, though, a surprisingly good agreement between experiment and theory is found. All of this rationalizing of experiment with theory presupposes that the experimental ee's are related only to the differences in energy between the diastereomeric transition states. This assumption does not consider the possibility of alkylation in the absence of catalyst, stereochemically ineffective alkylation involving catalyst degradation products, or racemization of the product, all of which would decrease the level of asymmetric induction.

IV. Intermolecular Forces. One problem with comparing *si* vs *re* selectivities from simple energy minimization is that a large number of minima on the hypersurface of the supermolecule exist and it is not possible to know whether the global minimum has been obtained. Another problem is that a single energy structure is not especially meaningful; a statistically averaged structure would be more useful. An attempt was made to obtain such a structure by molecular dynamics. Short MD simulations for *si* and *re* face complexes were conducted. A statistically averaged energy was determined by collecting a large number of structures during the simulation, Boltzmann weighting them to determine their probabilities, and then multiplying their energies by this weighting factor.

The first study was on the *si* and *re* faces of the *tert*-butyl *Z* enolate **3Z**. The previously optimized system was warmed to 300 K for 1 ps and equilibrated for 4 ps at 300 K. This was followed by a production run of 5 ps to sample configurations for the statistical mechanics. During these simulations it was noted that the enolates move far from their equilibrium positions. It became clear that very long simulation times would be needed for the complete analysis and, given the number of enolates to be evaluated, this became a computationally intractable problem. Considering the shallowness of the intermolecular potential energy surfaces described earlier, these results are not surprising. Consequently, the goal of attaining averaged values was abandoned and only the energy-minimized structures were considered. Furthermore, the discussion is restricted to only the Merck and *Z* enolates because these ions correlate nicely with experimental results.

a. Component Energies. Empirical force fields, as implemented in molecular mechanics, assume the total energy to be the sum of contributions from various component terms, $E = E_s + E_b + E_w + E_{vdw} + E_{other}$.[26] It was wondered if, hidden amongst the component energies of this series of closely related molecules, a pattern or a trend could be observed. Consideration of the MM2 component energies for *si*- and *re*-face structures (Table SVIII, supplementary materials) does not lead to any apparent trends. Usually the more stable face has the lower coulombic energy (most attractive) but this is not always true. The only thing that can be said about the ion pairs is that they are tightly held together by coulombic interactions. Clearly, there is a subtle interplay between coulombic attractions and steric repulsions in these complexes.

The next trend or pattern searched for was a structural one (e.g., does the more stable facial binding always result in one docking orientation while the other face result in another orientation?). This was accomplished by looking at the angle of the projection (17) of the enolate vector

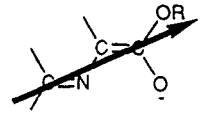

16

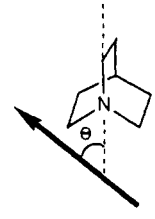

17

described by **16** onto the front face of the catalyst (Table SIX, supplementary materials). Again, there are no apparent trends. It is not clear whether the lack of orientational trends is because they simply do not exist or because the structures being used are not averaged ones.

b. Fragment Energies. As enolates associate with the cinchoninium ion they form weakly bound ion pairs. It is imperative to know which parts of the catalyst are most responsible for binding of enolate ions. Likewise, it is important to know which part(s) of the enolate ions are most responsible for binding to the catalyst. With molecular mechanics, where the interatomic interactions are computed pairwise-additive, all of one molecule is interacting with all of another. To address, in a quantitative and nonbiased way, which groups are most responsible for complexation an algorithm has been developed[28] that allows partitioning of the total binding energy (enthalpy only) into molecular fragments. The intermolecular energy is a dynamical value that has been derived by sampling all the configurations of the system over an infinite time period (the 155 000 unique samples described in Methodology). The binding energy being partitioned accounts, in a statistically averaged way, for the probability of finding the enolate at a latitude θ and longitude ϕ and the likelihood of the enolate having a particular orientation with respect to the catalyst. Those structures in the low-energy

(26) Burkert, U.; Allinger, N. L. *Molecular Mechanics*; ACS Monograph Series; American Chemical Society: Washington, DC, 1982.
(27) Lipkowitz, K. B.; Baker, B. *Anal. Chem.* **1990**, *62*, 770–774.
(28) Lipkowitz, K. B.; Baker, B.; Zegarra, R. *J. Comput. Chem.* **1989**, *10*, 718–732.

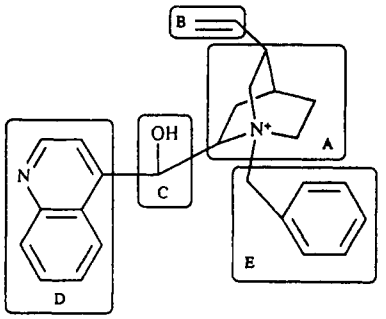

2

Figure 11. Definition of catalyst fragments.

Table IV. Percent Contribution Catalyst Fragments Make toward Binding *Z* Enolates 3*Z*–9*Z* and Merck Enolate 10

enolate	%A	%B	%C	%D	%E
3*Z*	63.63	-1.19	7.45	0.12	29.99
4*Z*	67.46	-1.07	6.26	-1.41	28.73
5*Z*	64.71	-1.12	8.31	-1.66	29.76
6*Z*	66.48	-0.99	6.56	-1.03	28.98
7*Z*	67.67	-0.42	6.82	-0.08	26.01
8*Z*	66.16	-0.99	7.83	-0.98	27.98
9*Z*	66.52	-0.65	6.95	-0.59	27.78
10	78.77	-1.71	2.72	-0.55	20.83

front-side regions around the catalyst are more likely to occur than other structures and are weighted accordingly in the analysis.

i. Catalyst. The *N*-benzylcinchoninium ion (2) is divided into five fragments that have been arbitrarily assigned based on established functional groups (Figure 11). The contribution fragments A–E make toward the binding of *Z* enolates 3–9 and the contributions these same fragments make for binding the Merck enolate 10 are given in Table IV. These results represent a Boltzmann weighted macroscopic view of what each portion of the catalyst "feels" or "senses" as the enolate binds to it.

The groups most responsible for binding are the quinuclidine fragment, the benzylic fragment, and the hydroxyl fragment in that order, while the vinyl group and quinoline ring are of lesser importance (close to zero or a slightly repulsive contribution). For all benzophenone imine *Z* enolates considered, the average percent contribution to the total binding energy of fragments A–E are as follows: 66% (±4%), -1% (±1%), 7% (±2%), -1% (±2%), and 29% (±4%), respectively. For the Merck enolate the partitioning of binding energies for fragments A–E are as follows: 79%, -2%, 3%, -1%, and 21%, respectively. It is interesting to note the small deviation in fragment contribution from enolate to enolate, even when considering the Merck enolate.

These results can be interpreted in the following way. The binding originates from fragments C (as hydrogen bonding) and from fragments A and E (as coulomb attractions). The positive charge on the catalyst is dispersed over these latter two groups. The vinyl group and the quinoline actually tend to repel the substrate as the enolates associate with the positive charge. The vinyl group, being on the rear side of the catalyst is, therefore, useless with regard to asymmetric induction. The quinoline ring, however, plays a key role, although it is not responsible for binding. Its function is to serve as a pedestal onto which the planar enolates can step. These insights point to fragments A, C, and E for synthetic modification. These studies are in progress and will be reported at a later date.

ii. Enolate. Enolates 3–9 were partitioned into five fragments, and the Merck enolate 10 was divided into four

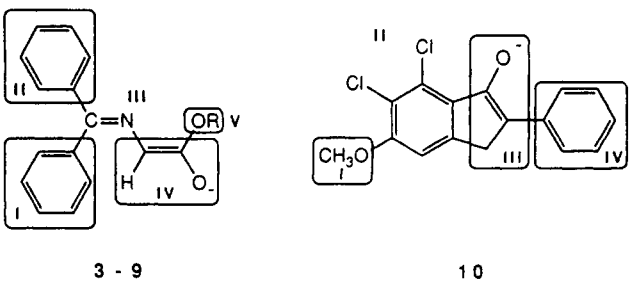

3 - 9 10

Figure 12. Definition of enolate fragments.

Table V. Percent Binding Energies Attributable to Fragments on *Z* Enolates 3*Z*–9*Z* and Merck Enolate 10

enolate	%I	%II	%III	%IV	%V
3*Z*	12.82	17.13	27.77	27.57	14.71
4*Z*	14.36	14.33	26.95	28.64	15.74
5*Z*	11.81	16.84	27.03	28.84	15.49
6*Z*	13.96	14.67	27.06	28.66	15.65
7*Z*	13.30	13.80	27.08	28.34	17.48
8*Z*	13.17	16.10	27.28	28.28	15.18
9*Z*	11.43	14.46	26.38	29.49	18.24
10	7.18	27.89	43.38	22.50	

fragments (Figure 12). What each imine enolate fragment "senses" as it slides over the van der Waals surface of the catalyst is presented in Table V. Again, there is relatively little variation from enolate to enolate. Most of the attractive interactions come from fragments III and IV. The results of the Merck enolate are also provided in Table V. Most of the attractive interactions originate from fragment III, the enolate portion, which is consistent with the other enolates and chemical intuition.

Summary

The objective of this research was to consider where the enolate binds to the catalyst and what forces are at play holding the complex together and to discern how enantioselection takes place. All of this has been considered in spite of the ambiguity of *Z*–*E* enolate configuration. Several insightful conclusions can be drawn.

First, the minimum-energy structure of the catalyst was similar to but not the same as that found from X-ray crystallography; the major difference is found in the orientation of the vinyl group, which adopts a more compressed orientation in the crystal than that in the gas or liquid states. The distribution of conformational states accessible to the catalyst at 300 K was also assessed (see supplementary material). It is concluded that the vinyl group on the rear side of the molecule is freely rotating with no preferred orientation. The rest of the molecule looks like the crystal structure. Both static and dynamical views of the benzylcinchoninium ion indicate the molecule inherently wants to adopt a shape where the aromatic rings are essentially coplanar with one another and orthogonal to the 3-fold axis of the quinuclidine. These results support the proposed alkylation mechanism of the Merck group.

Second, it is found that the most likely binding region for all enolates is on the front side of the *N*-benzylcinchoninium ion as proposed by the Merck group.[13b] Generally speaking, the intermolecular potential energy surfaces are flat with gently rolling hills and wide valleys interconnecting minima. This suggests wide amplitude sliding motions in the ion pairs. Solvent and temperature effects should therefore be important in these asymmetric alkylations.

Third, it is observed that the predominant forces holding the complexes together are coulombic. Most important

in this regard is the fact that the charges are highly dispersed. The anion has several negatively charged sites competing with each other for binding to the cation. Attenuating this is the fact that the ammonium center is deeply sequestered within the catalyst and its positive charge is significantly delocalized. These delocalized charges give rise, in part, to the broad and shallow minima on the intermolecular potential surfaces, and they cause problems with regard to orientation of the enolate vector when it does bind to catalyst. It is recommended that functionality localizing rather than delocalizing charge on the enolate be considered in future synthetic work.

Fourth, while transition states leading to *R* vs *S* product were not modeled, it was possible to successfully model the facial selectivity of enolate binding to catalyst when the inherently less stable *Z* enolate 12 binds. Thus, it is proposed that the active enolate has the *Z* configuration. By use of our search strategy, it was possible to correctly predict which face binds to the catalyst for the seven *Z* enolates. Furthermore, a linear relationship between ΔE, the energy difference between *si* vs *re* facial selectivity, and experimental ee is found. Hence, theory and experiment are consonant.

Fifth, it was not possible to discern any trends or patterns that explain the origins of enantioselectivity. The reason for this is thought to be the use of single energy-minimized structures rather than those that have been averaged in a statistically meaningful way. Nonetheless, this modeling is now of value because the enantiomeric excess expected for as yet untested enolates can be predicted.

Finally, using a unique energy partitioning algorithm, it was possible to determine what each fragment senses in the ion pair for both catalyst and enolate. For the catalyst, fragments A, C, and E are responsible for most of the binding. The vinyl group is found to play no role in asymmetric induction but the quinoline ring plays a critical role (in spite of not contributing to the binding of enolate) by serving as a platform onto which the enolates rest in their efforts to associate with the other fragments. The catalyst, in turn, is attracted primarily to fragment III and IV in the benzophenone series and to fragment III in the Merck enolate. Overall, the depiction by the Merck group[13b] of the shape and type of ion pairing interactions that takes place with enolates and catalyst are in agreement with the modeling studies presented here.

Acknowledgment. This work was supported in part by a grant from the National Science Foundation (CHE-8901828), by the Petroleum Research Fund, administered by the American Chemical Society, and gracious support from Kris Froehlke and the IUPUI Computing Services. We also thank Clark Still and Kevin Gilbert for preliminary releases of their programs and the Merck group for kindly providing unpublished X-ray data.

Supplementary Material Available: Materials describing the results of MD simulations of catalyst along with contour plots of enolate–catalyst intermolecular potential energy surfaces, tables of conformational energies and torsion angles for *Z* and *E* enolates 3–9, MM2 component energies of the lowest energy ion pairs, and the projected angles of enolate vector 16 onto catalyst (23 pages). Ordering information is given on any current masthead page.

Synthesis of 2,5-Substituted Piperidines and Their Bicyclic Piperazine Analogues: The 2,7-Substituted Octahydro-2*H*-pyrido[1,2-*a*]pyrazines

Frans Compernolle, M.-Ashty Saleh, Suzanne Toppet, and Georges Hoornaert*

Laboratorium voor Organische Synthese, K.U.Leuven, Celestijnenlaan 200 F, B-3030 Leuven-Heverlee, Belgium

Received February 26, 1991

Partial and complete reduction of the key compound 1-benzyl-5-(ethylenedioxy)-2-piperidinecarbonitrile (1) was applied to generate the corresponding aldehyde 2 and primary amine 3. These were transformed into bicyclic 7-(ethylenedioxy)-2(*R*)-octahydro-2*H*-pyrido[1,2-*a*]pyrazines 7 (R = H) and 15 (R = aryl) through the following sequence: (i) chloroacetylation of 3 and of arylamines derived from 2, (ii) cyclization to give the intermediate lactams 5 and 14, and (iii) reduction with $LiAlH_4$. Deprotection of the *N*-aryl compounds 15 yielded the corresponding ketone model compounds 16. From amino acetal 7, a complementary ketone synthon 11 was prepared via N-benzylation and cleavage of the acetal group, providing a general route to piperidine-bridged analogues of 1,4-substituted piperazine drugs.

Recently, we reported[1] the synthesis of 1-benzyl-3-(ethylenedioxy)-2-piperidinecarbonitrile (1), which was obtained via regioselective Hg^{2+} oxidation and trapping of the resulting iminium ion with cyanide. The versatility of synthon 1 in the preparation of 2,5-substituted piperidines was demonstrated by its conversion to the α-anion and further reaction with electrophiles. Here, we describe reduction of 1 to the corresponding aldehyde and primary amine, both of which served as intermediates in the synthesis of bicyclic piperazine analogues of 2,5-substituted piperidines. Whereas some members of the resulting product class, i.e., the octahydro[1,2-*a*]pyrazines have been described already,[2] the 2,7-substituted analogues are reported here for the first time. This 2,7-substitution pattern can be used to define the "active conformations" of monocyclic 1,4-substituted piperazine drugs.

Reduction of aminonitrile 1 with $LiAl(OEt)_3H$ afforded the crude aldehyde 2 in about 70% yield based on weight

(1) Compernolle, F.; Saleh, M. A.; Toppet, S.; Van den Branden, S.; Hoornaert, G. *J. Org. Chem.*, in press.

(2) Cheeseman, G. W. H.; Cookson, R. F. In *The Chemistry of Heterocyclic Compounds*, Vol. 35 Condensed Pyrazines; Weisberger, A., Taylor, E. C., Eds.; Wiley Interscience: New York, 1979; Chapter XXVII, p 463.

0022-3263/91/1956-5192$02.50/0